Chinese Chemical Letters 33 (2022) 2117–2120

Contents lists available at ScienceDirect

Chinese Chemical Letters

journal homepage: www.elsevier.com/locate/cclet

Water-induced luminescence improvement in a lanthanide β-diketone complex for monitoring water purity

Xiaojun Zhang, Xiaomeng Jin, Yuxin Li*

Key Laboratory of Function Inorganic Material Chemistry (MOE), School of Chemistry and Material Science, Heilongjiang University, Harbin 150080, China

ARTICLE INFO

Article history:
Received 29 May 2021
Revised 7 August 2021
Accepted 17 August 2021
Available online 21 August 2021

Keywords:
Water-induced luminescence improvement
Lanthanide complex
β-Diketone ligand
Water quality monitor
Luminescence sensing
Through-space charge transfer

ABSTRACT

Water-caused luminescence quenching is a well-known and intractable issue for luminescence lanthanide complexes, greatly confining their broad application as sensing and displaying devices in water system. Herein, an anionic and coordination-saturated lanthanide complex with a nanosheet-like structure has been prepared. It exhibits excellent photophysical properties both in solid state and in aqueous suspension. Noteworthily, a 13% improvement for sensitization efficiency from organic ligand to central lanthanide ion has been realized, indicating an exceptional phenomenon of water-induced luminescence improvement which is rarely reported previously. Moreover, the aqueous suspension of as-prepared luminophore could act as a chemo-sensor responding to various organic solvents in water. Both of water-induced luminescence improvement and extended sensing behavior in this work provide a new platform for developing highly performant and practical luminescent materials in the water system.

Lanthanide complexes are crystalline hybrid materials assembled by trivalent lanthanide (Ln^{3+}) ions and organic ligands [1–3]. Benefiting from the antenna effect, characteristic luminescence of Ln^{3+} ions, especially Eu^{3+} and Tb^{3+} ions, are well sensitized by the light-harvesting ligands *via* a series of energy transfer processes [4–6]. These complicated photoluminescence pathways determine the sensitive nature to circumstance details, thereby providing an effective platform for chemically responding to metal cations, oxoanions, organic solvents, and biomolecules [7–10]. However, it is commonly believed that luminescent lanthanide complexes are unsuitable for water-bearing systems, because the stretching vibration of hydroxyl groups in water molecules confines the energy transfer process from the triplet state of ligand to the receiving energy level of Ln^{3+} ions, leading to dramatic luminescence quenching [11–13]. This greatly limits the practicality of lanthanide-based luminescence complexes. Therefore, it is meaningful, though challengeable, to develop a water-stable even water-improving luminescence lanthanide complex.

Enhancing hydrophobicity of luminophores and thereafter inhibiting the immediate contact with solvent water molecules is a potential mean to settle the above-mentioned water-induced luminescence quenching issue [14]. Based on this consideration, $(HNEt_3)^+[Eu(DBM)_4]^-$ (briefly as Eu-DBM, DBM = dibenzoylmethane) is selected as a luminophore (Figs. S1 and S2 in Supporting information) [15]. Firstly, its phenyl-surrounding outside surface provides strong hydrophobicity. Secondly, it has coordination-saturated lanthanide centre, which could decrease the impact of coordination solvent molecular replacement and further weaken the water-induced effect to lanthanide luminescence. Thirdly, its anionic framework is helpful to the dispersibility in polar solvents such as water. Therefore, in this work, the Eu-DBM material is selected as a luminophore to study its potential on water-induced luminescence improvement. For further enhancing the dispersibility and stability, the nanosheet-like Eu-DBM material is also prepared. Then, its application on sensitive detection toward extended organic solvents in water has been investigated.

A top-down strategy was utilized to prepare the Eu-DBM nanosheet by two facile steps. The bulky crystal of Eu-DBM was firstly prepared in terms of a previous method [15]. It was then exfoliated into nanosheets under 720 W ultrasonication for 24 h at room temperature. Atomic force microscopy (AFM) image revealed its two-dimensional (2D) sheet-like morphology with a height of uniform 12 nm (Fig. 1a). Scanning electron microscopy (SEM) image further confirmed a sheet-like appearance with the size of 100–200 nm (Fig. 1b). Fourier transition infrared (FT-IR), ultraviolet-visible absorption (UV-vis) thermogravimetric differential thermal analysis (TG-DTA) spectra, and the powder X-ray diffraction pattern of the Eu-DBM nanosheet held similar patterns with those of bulky ones reported previously (Figs. S3–S6 in Supporting information) [15]. Furthermore, elemental mapping analysis further proved the composition consisted of C, O and Eu el-

* Corresponding author.
E-mail address: liyuxin@hlju.edu.cn (Y. Li).

https://doi.org/10.1016/j.cclet.2021.08.080
1001-8417/

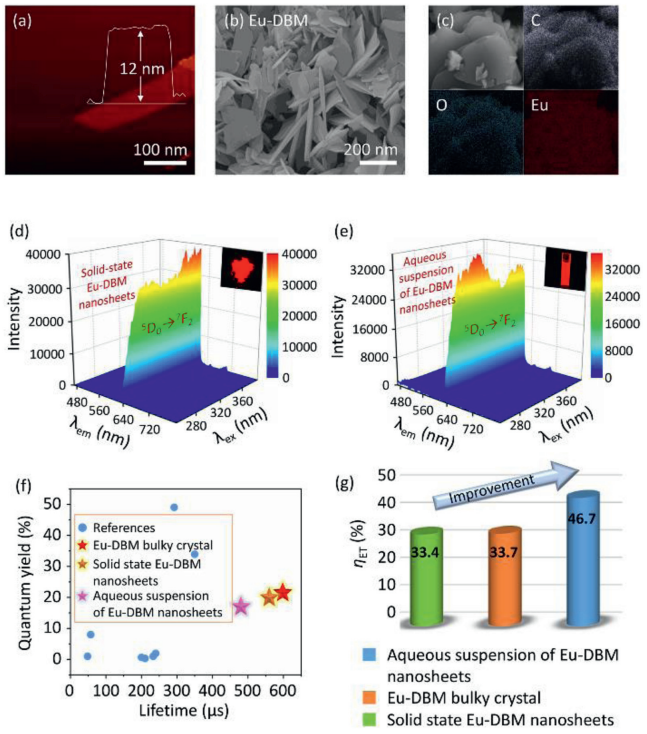

Fig. 1. AFM (a), SEM (b), and elemental mapping (c) images of Eu-DBM nanosheets. 3D photoluminescent spectra of Eu-DBM nanosheet in solid state (d) and in aqueous solution (e). (f) Comparison of lifetime and quantum yield in this work with previous reports. (g) Comparison of Eu-DBM bulky crystal and nanosheet in solid state and in aqueous suspension.

ements (Fig. 1c). Elementary analysis, X-ray photoelectron spectroscopy (XPS), and energy disperse spectroscopy (EDS) presented an agreeable proportion of elements with crystallographic data (Table S1 in Supporting information) [15]. These results indicated that the obtained Eu-DBM nanosheets had the same structure and composition as their bulky crystals.

The three-dimensional (3D) photoluminescence (PL) spectra of Eu-DBM nanosheet exhibited strong emission at 614 nm throughout the excitation from 250 nm to 390 nm, rendering stable and intense red-light emission with the Commission Internationale de L'Eclairage (CIE) coordination of (0.648, 0.330) (Fig. 1d and Fig. S7 in Supporting information). This excitation-wavelength independence in such a broad range was rarely reported in the luminescence lanthanide complexes [12,13]. The unsplit band at 614 nm implied a highly symmetric structure of the Eu-DBM complex [16]. The electric dipole transition ($^5D_0 \rightarrow {}^7F_2$) at 614 nm was approximately 22-fold stronger than the magnetic one ($^5D_0 \rightarrow {}^7F_1$) at 592 nm, indicating the highly symmetric coordination environment of central Eu^{3+} ion in the complex [17]. Noteworthily, after dispersing the Eu-DBM nanosheet in water, the 1 g/L suspension presented the nearly same 3D PL contour as the solid-state one, exhibiting the strong red-light emission (Fig. 1e). The time-dependent curve showed that the luminescent intensity at 614 nm could remain at least 24 h with a < 5% declination (Fig. S8 in Supporting information). This excellent stability originated from the good dispersibility of the complex nanosheets in water.

The presence of strong Eu^{3+} characteristic luminescence and the absence of DBM ligand fluorescence suggested an effective antenna effect in the Eu-DBM complex: the adsorbed UV light by DBM ligand could effectively transfer to the Eu^{3+} ion, and then sensitize its characteristic luminescence. To confirm this hypothesis, the sensitization efficiency (η_{ET}) was subsequently calculated in terms of the following equations Eqs. 1–3 [18–20].

$$\eta_{ET} = \frac{\Phi_{overall}}{\Phi_{Ln}} \quad (1)$$

$$\Phi_{Ln} = \frac{\tau_{obs}}{\tau_{rad}} \quad (2)$$

$$\frac{1}{\tau_{rad}} = A_{MD,0} n^3 \left(\frac{I_{tot}}{I_{MD}}\right) \quad (3)$$

According to Eq. 1, $\Phi_{overall}$ was the overall luminescence quantum yield measured by the integrated sphere method (Table S2 in Supporting information). Φ_{Ln} was the intrinsic quantum yield of the lanthanide luminescence, obtained in terms of Eq. 2, where the observed lifetime (τ_{obs}) was determined by monitoring the emission decaying curve within the $^5D_0 \rightarrow {}^7F_2$ transition at 614 nm (Figs. S9–S11 in Supporting information). The calculated radiative lifetime (τ_{rad}) could be calculated through Eq. 3, where $A_{MD,0}$ was the spontaneous emission probability of the magnetic dipole transition and equated to 14.65 s^{-1} for Eu^{3+} ion ($^5D_0 \rightarrow {}^7F_1$); n represented the refractive index of the tested sample (n equated to 1.55 for solid-state Eu-DBM and 1.33 for Eu-DBM nanosheets aqueous suspension); I_{tot} and I_{MD} were the integrated emission of the total $^5D_0 \rightarrow {}^7F_J$ transition and the $^5D_0 \rightarrow {}^7F_1$ transition, respectively. As a result, the Eu-DBM bulky crystal and nanosheet in solid state and in aqueous suspension exhibited high τ_{obs} and $\Phi_{overall}$ values, surpassing most of the reported luminescent lanthanide complexes and nearly all the Eu-DBM-based complexes (Fig. 1f). Compared with the solid-state Eu-DBM, the 1 g/L aqueous suspension of Eu-DBM nanosheets showed only slight declination on τ_{obs} and $\Phi_{overall}$ (Table S2 and Figs. S9–S11). Noteworthily, the η_{ET} in Eu-DBM aqueous suspension was calculated as 46.7%, a 13.0% and 13.3% improvement compared with that of the bulky crystal and solid-state nanosheets (Fig. 1g). This improvement on sensitization efficiency states the increasing energy transfer from the DBM ligand to the central Eu^{3+} ions. In other words, the water solvent improved the luminescence of Eu^{3+} ion, realizing the water-induced luminescence improvement which is rarely reported previously (Table S2).

The mechanism of this water-induced luminescence improvement in the Eu-DBM complex was then explored. Firstly, the Eu-DBM was dispersed in various common solvents to prepare 1 g/L solution or suspension. As seen in Fig. 2a, the complex exhibited poor solubility in water but good in nearly all other common organic solvents. This derived from the strong hydrophobic property due to the phenyl-surrounding outside surface of Eu-DBM. Comparatively, the aqueous suspension of the Eu-DBM nanosheets presented strong and uniform red-light-emission of characteristic Eu^{3+} ion (Figs. 2b and c). However, the Eu-DBM solution in various common organic solvents was obviously quenched. These excellent and unorthodox photophysical properties of Eu-DBM in water system could attribute to the insolubility and aggregation state which avoided the immediate contact between water molecules and the central Eu^{3+} ions. Secondly, given that water possesses the highest surface tension and polarity among all solvents, it could suppress surficial phenyl groups and yield structural modification. According to Fig. S5, the PXRD pattern of the Eu-DBM nanosheet had strong peak at 7.0°, which indicated that the (200) plane was exposed to water solvent, as shown in Fig. 2d. The strong surface tension of solvent water molecules could compress the hydrophobic phenyl groups inward, resulting in the more planarity between the neighboring phenyl and carbonyl groups. This enhanced the π-π conjugation and suppressed the stretching vibration of the C–C bond of benzene rings. After the benzene rings are fixed, the energy loss caused by the vibration of the chemical bonds were reduced, making the more effective sensitization of Eu^{3+} ions (Fig. 2d). Moreover, the dihedral angle and distances between

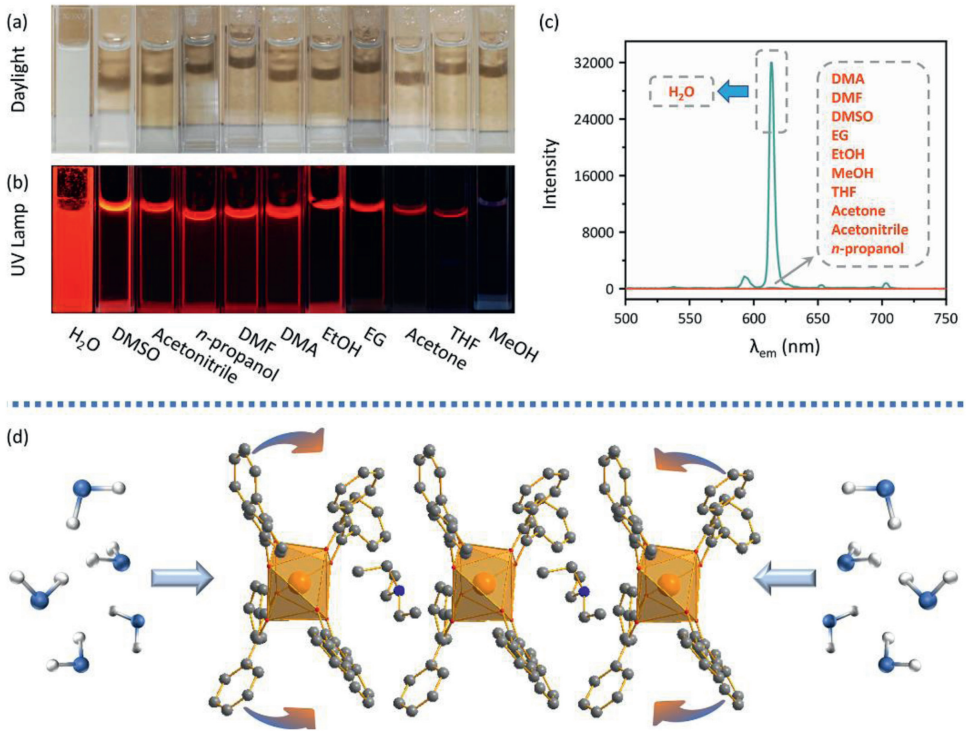

Fig. 2. Photo images of Eu-DBM samples in various solvents under daylight (a) and UV lamp (b). Photoluminescent spectra of Eu-DBM samples in various solvents upon the excitation of 304 nm (c). Mechanism of water-induced luminescence improvement (d).

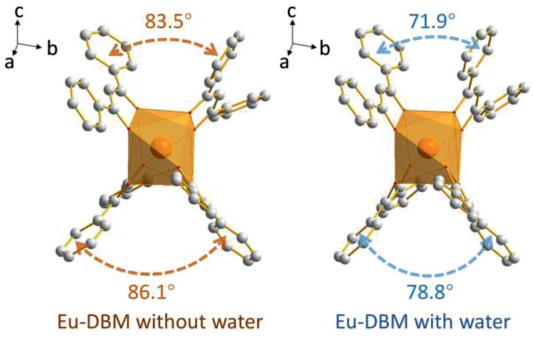

Fig. 3. Geometrically optimized structure of Eu-DBM without water (left) and with water (right). H and $(HNEt_3)^+$ have been transparentized.

neighboring phenyl/carboxyl planes was decreasing after putting Eu-DBM nanosheets into water environment, which promoted the through-space charge transfer (TSCT) process [21–23]. To prove this hypothesis, the Eu-DBM molecule in the water environment was geometrically optimized by theoretical calculation by using Material Studio 8.0 software with GGA/BLYP basis set [24]. As shown in Fig. 3, under the effect of the water molecule, a more planarity between phenyl and carbonyl groups could be observed. The dihedral angle between the neighboring phenyl/carbonyl planes were also reduced by 11.6° and 7.3°, respectively, compared with the original structure. This confirmed that the water-induced luminescence improvement primarily resulted from the TSCT process as discussed above.

Considering that the as-prepared Eu-DBM nanosheet presented excellent luminescence improvement in water and obvious quenching in other organic solvents, it could act as a luminescence sensor toward extensive organic solvents in water, being an indicator to monitor water purity. Based on this, various organic solvents were gradually titrated into 1 g/L Eu-DBM aqueous suspension. By monitoring their luminescence intensity at 614 nm upon the 304 nm excitation, the relationship between volume proportion (v/v) and quenching efficiency was depicted in Figs. 4a and b. The luminescence intensity dramatically decreased upon the addition of various organic solvents. When the volume proportion of added organic solvent was approximate 2.5%, the luminescence intensity dropped by about 50%. In other words, the nanosheets exhibited similar and sensitive changes in luminescence intensity toward nearly all organic solvents. To the best of our knowledge, this colligative property toward such extensive sensibility was rarely reported and applicable for water purity monitor. As shown in Figs. 4c–l, the Eu-DBM aqueous suspension turned to be more pellucid as the gradual addition of various organic solvents. The luminescent intensity observed by naked eyes also presented an obvious decrease under the 365 nm UV lamp.

Then, we quantitatively examined the luminescent quenching coefficient (K_{SV}) of the Eu-DBM sensor toward various organic solvents in water *via* the distinguished Stern-Volmer (SV) equation: $I_0/I - 1 = K_{SV} \times [C]^n$, where I_0 and I were the luminescent intensity before and after adding analytes, and [*C*] was the molar concentration of the analyte [25,26]. The parameter n equalled to 1 when the SV curve displayed a linear relationship. According to Figs. S12–S31(Supporting information), the SV curve of the Eu-DBM sensor displayed a linear relationship in the concentration range of 0–0.6 mol/L toward DMA, DMF, DMSO, EtOH, MeOH, acetonitrile, and n-propanol, but a distinct curvature toward THF, acetone, and ethylene glycol (EG). The calculated K_{SV} values were in order of acetone (8.85 L/mol) > THF (7.35 L/mol) > DMF (7.22 L/mol) > EtOH (6.54 L/mol) > *n*-propanol (4.79 L/mol) > acetonitrile (2.54 L/mol) > MeOH (2.52 L/mol) > DMA (2.78 L/mol) > DMSO (2.43 L/mol) > EG (2.11 L/mol). Subsequently, the limitations of detection (LODs) were calculated *via* the formula of $3\sigma/K_{SV}$, where σ is the standard deviation of the luminescent intensity for five-time blank measurement at 2 min intervals [27–30]. As a result, the LODs toward various organic solvents ranged from 4.07×10^{-4} mol/L to 1.43×10^{-3} mol/L. In order to improve the detection convenience, the relationship between the volume ratio of the 10 organic sol-

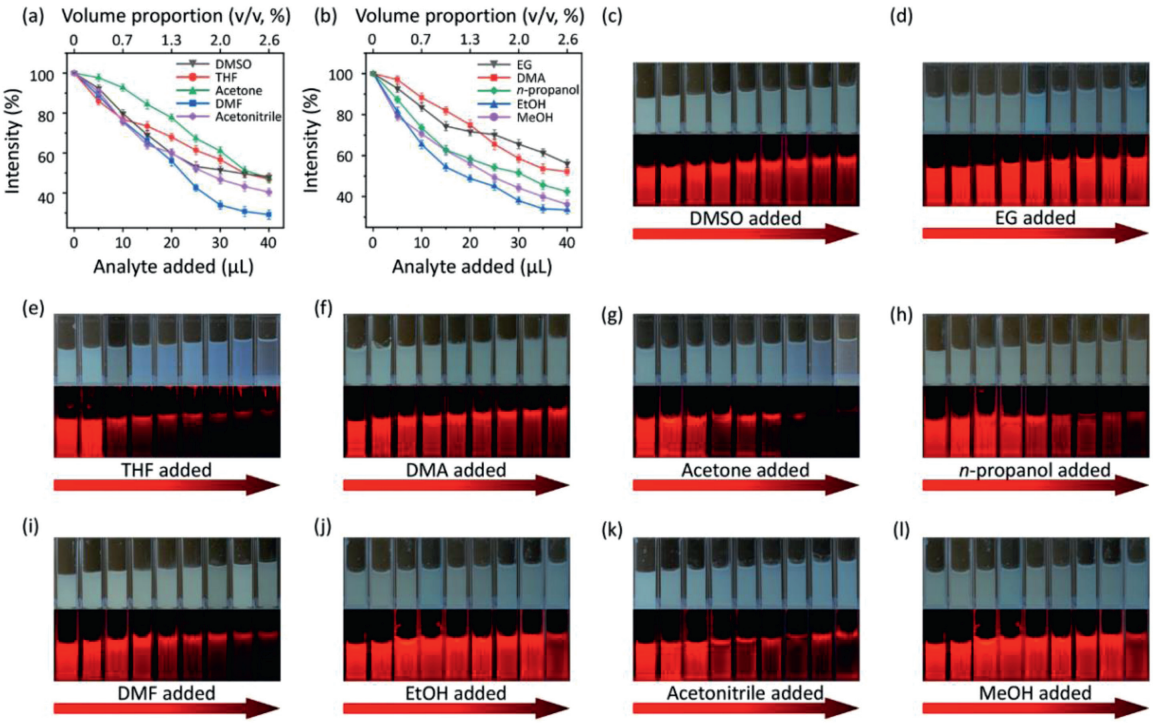

Fig. 4. (a, b) Relationship between the relative luminescent intensity of Eu-DBM sensor and the added quantity of organic solvents. Photo images under daylight and UV lamp of Eu-DBM sensor upon adding DMSO (c), EG(d), THF (e), DMA (f), acetone (g), n-propanol (h), DMF (i), EtOH (j), acetonitrile (k) and MeOH (l).

vents and the relative luminescence intensity was averaged and the polynomial fitting was performed (Fig. S32 in Supporting information). The relationship between them is approximately fitted as $y = 5.23x^2 - 35.47x + 100.00$ and $R^2 = 0.999$. This extensive sensibility toward nearly all organic solvents in water demonstrated that the as-prepared Eu-DBM nanosheets could be utilized to ratiometrically determine the organic solvents in water. In addition, the sensor could be regenerated and reused for at least five cycles by centrifugation of the solution after use and washing several times with water (Figs. S33–S42 in Supporting information).

In conclusion, the water-stable Eu-DBM nanosheets exhibited exceptional water-induced luminescence improvement phenomenon, with a 13% improvement for sensitization efficiency. This attributes to the combined effect of hydrophobic-caused aggregation and through-space charge transfer in the water environment. Moreover, the well-dispersed aqueous suspension of Eu-DBM nanosheets could act as a luminescence sensor which responses to trace organic solvents in water, with good universality and recyclability. In this work, the water-induced luminescence improvement and extensive sensibility toward organic solvents in water were rarely reported previously in lanthanide-based materials. The successful development of this material provided a new platform for luminescent sensors in the water system, being practical values on monitoring water quality.

Declaration of competing interest

The authors declare that they have no known competing financial interests or personal relationships that could have appeared to influence the work reported in this paper.

Acknowledgments

We thank the National Natural Science Foundation of China (No. 22075071), and Reform and Development Fund Project of Local University supported by the Central Government.

Supplementary materials

Supplementary material associated with this article can be found, in the online version, at doi:10.1016/j.cclet.2021.08.080.

References

[1] C.D. Deng, Y.J. Qiao, Q.D. Chen, X.H. Shen, Chin. Chem. Lett. 28 (2017) 19–23.
[2] F. Saraci, V. Quezada-Novoa, P.R. Donnarumma, A.J. Howarth, Chem. Soc. Rev. 49 (2020) 7949–7977.
[3] J. Ma, T. Wang, C. Liu, H. Li, Chin. Chem. Lett. 29 (2018) 321–324.
[4] T. Zhang, Y. Liu, B. Hu, et al., Chin. Chem. Lett. 30 (2019) 949–952.
[5] W.Y. Sun, H.F. Lu, D.X. Wang, S.Y. Feng, Chin. Chem. Lett. 20 (2009) 1085–1087.
[6] M. Hasegawa, A. Ishii, Coord. Chem. Rev. 421 (2020) 213458.
[7] J. Zhou, H. Li, H. Zhang, et al., Adv. Mater. 27 (2015) 7072–7077.
[8] X.Y. Ren, L.H. Lu, Chin. Chem. Lett. 26 (2015) 1439–1445.
[9] X. Xu, L. Feng, J. Li, et al., Chin. Chem. Lett. 30 (2019) 549–552.
[10] Y. Liu, Q.L. Shi, J.L. Yuan, Chin. Chem. Lett. 26 (2015) 1485–1489.
[11] M. Yu, Y. Xie, X. Wang, Y. Li, G. Li, ACS Appl. Mater. Interfaces 11 (2019) 21201–21210.
[12] Y. Li, S. Li, P. Yan, et al., Chem. Commun. 53 (2017) 5067–5070.
[13] P. Li, H. Li, Coord. Chem. Rev. 441 (2021) 213988.
[14] P. Wu, J. Wang, C. He, et al., Adv. Funct. Mater. 22 (2012) 1698–1703.
[15] S. Akerboom, M.S. Meijer, M.A. Siegler, W.T. Fu, E. Bouwman, J. Lumin. 145 (2014) 278–282.
[16] J.-M. Zhou, W. Shi, N. Xu, P. Cheng, Inorg. Chem. 52 (2013) 8082–8090.
[17] K. Binnemans, Coord. Chem. Rev. 295 (2015) 1–45.
[18] Y. Zhou, H. Li, T. Zhu, T. Gao, P. Yan, J. Am. Chem. Soc. 141 (2019) 19634–19643.
[19] J.C.G. Buenzli, A.S. Chauvin, H.K. Kim, E. Deiters, S.V. Eliseeva, Coord. Chem. Rev. 254 (2010) 2623–2633.
[20] M.H.V. Werts, R.T.F. Jukes, J.W. Verhoeven, Phys. Chem. Chem. Phys. 4 (2002) 1542–1548.
[21] J. Hu, Q. Li, X. Wang, et al., Angew. Chem. Int. Ed. 58 (2019) 8405–8409.
[22] J. Hu, Q. Li, S. Shao, et al., Adv. Opt. Mater. 8 (2020) 1902100.
[23] X. Wang, S. Wang, J. Lv, et al., Chem. Sci. 10 (2019) 2915–2923.
[24] F. Bu, R. Duan, Y. Xie, et al., Angew. Chem. Int. Ed. 2 54 (2015) 14492–14497.
[25] B. Qu, Z. Mu, Y. Liu, et al., Environ. Sci. 7 (2020) 262–271 Nano.
[26] W. Wang, Q. Gao, X. Li, et al., Chin. Chem. Lett. 30 (2019) 75–78.
[27] J. Qian, N. Cao, J. Zhang, et al., Chin. Chem. Lett. 31 (2020) 2925–2928.
[28] Y. Li, Y. Ban, R. Wang, et al., Chin. Chem. Lett. 31 (2020) 443–446.
[29] Y. Yang, L. Zhao, M. Sun, et al., Dyes Pigments 180 (2020) 108444.
[30] M. Sun, Y. Li, L. Zhao, et al., ACS Appl. Polym. Mater. 3 (2021) 2998–3008.